Dynamics of a capsule flowing in a tube under pulsatile flow

Jorge Maestre[a], Jordi Pallares[a,*], Ildefonso Cuesta[a], Michael A. Scott[b]

[a]*Departament d'Enginyeria Mecànica, Universitat Rovira i Virgili, Av. Països Catalans, 26, 43007 Tarragona, Spain.*
[b]*Department of Civil and Environmental Engineering, Brigham Young University, Provo, UT 84602, USA.*

Abstract

We analyze numerically the behavior of a deformable micro-capsule confined in a pipe under a pulsatile flow. The capsule moves and is deformed by the action of a pulsatile flow inside the tube with a non-null mean velocity. This configuration can be found in the nature and in many bioengineering systems where artificial capsules are driven by micro-pumps through micro-channels. The capsule is considered as a thin hyperelastic membrane, which encloses an internal fluid. As it has been demonstrated in the literature, this model represents a wide range of artificial capsules, for example, the alginate-based capsules, typically used in bioengineering applications. A hybrid isogeometric finite element method and boundary element method based on a T-spline discretization and formulated in the time domain is used to solve the mechanical and hydrodynamical equations. The influence of the relative rigidity of the membrane, frequency and amplitude of the pulsatile flow is studied. Results show that the behavior of the capsule differs from steady flows and it depends strongly on the frequency of the flow and mechanical characteristic of the capsule.

Keywords: Deformable capsule, Pulsatile flow, IGA, T-spline

1. Introduction

The dynamics of deformable capsules suspended in external flows has been intensively investigated during the last decades because of the related multiple biological and industrial applications. A capsule is a liquid enclosed by a deformable membrane. The membrane acts as a protector, preventing the deterioration of the internal substance by the action of exterior agents, and it facilitates its transport. Erythrocytes (or red blood cell, RBC) and leucocytes, present in the blood, are examples of biological capsules. The deformability of these cells is fundamental for their circulation through micro-vessels. Nowadays, artificial micro-capsules are being used for sophisticated therapeutic treatments such as drug delivery (see Bansode et al. (2010)). This technique is known as micro-encapsulation and it is also being investigated and used in other areas such as the cosmetic and food industries (see Casanova & Santos (2016)). The analysis of the dynamics of capsules is crucial to the understanding of biological phenomenon as well as for the design of bio-artificial capsules and development optimization of new bioengineering applications.

The motion and deformation of capsules in suspended flows involve complex fluid-structure interactions. Thanks to the progress in computing capacity, numerical simulations have become a powerful tool to study this problem. Different numerical models have been proposed in the literature. In most of these models, the capsule is considered as an extremely thin elastic membrane filled with an internal incompressible Newtonian liquid (e.g. Ramanujan & Pozrikidis (1998); Diaz & Barthès-Biesel (2001); Barthès-Biesel et al. (2002); Lac et al. (2004); Lac & Barthès-Biesel (2005); Lefebvre & Barthès-Biesel (2007); Doddi & Bagchi (2008); Dodson III & Dimitrakopoulos (2009); Walter et al. (2010)). This model has been demonstrated to represent satisfactorily a wide range of artificial capsules (see Pieper et al. (1998); Carin et al. (2003); Husmann et al. (2005); Lefebvre et al. (2008); Chu et al. (2011)). Regarding this aspect, it is interesting to note the work presented by Lefebvre & Barthès-Biesel (2007), who showed a comparison between experimental observations and numerical simulations of an alginate covalently linked to human serum albumin capsules flowing in a pipe. The alginate-based compound is one of the most used biomaterials in

*Corresponding author.
Email address: jordi.pallares@urv.cat (Jordi Pallares)

micro-encapsulation applications due to its bio-compatibility (see Gonzalez-Pujana et al. (2018)). These authors used a bi-dimensional Skalak model of the membrane (Skalak et al. (1973)) and revealed a good agreement with experiments. Using also a bi-dimensional model of the membrane, Hu et al. (2012) proposed an inverse problem to infer the mechanical properties of artificial capsules from experimental measurements of the capsule deformation flowing in a channel. More sophisticated models have been developed recently, which also consider the effect of bending rigidity, viscoelasticity or rheology of the membrane. The reader is refered to Barthès-Biesel (2016) for a comprehensive and complete review of the capsule models.

Early studies of deformable artificial capsules in unbounded steady shear flows were presented by Pozrikidis and co-workers in Pozrikidis (1995, 2001, 2003); Ramanujan & Pozrikidis (1998). These authors analyzed the transient deformation of capsules with different initial shapes (spherical, oblate and biconcave), capillary numbers and viscosity ratio (between internal and external fluid viscosity). The numerical simulations show that an initial spherical capsule, under a steady shear flow, deforms into an elliptical shape and it reaches a steady inclination with respect to the flow direction while the membrane rotates around the internal fluid. This phenomenon is known as tank-treading and it has also been observed experimentally by Rehage et al. (2002); Fischer et al. (1978); Fischer & Schmid-Schönbein (1978). In the context of unbounded flows, several studies have been presented focused on different parameters, as the influence of different constitutive laws for the membrane (Lac et al. (2004)), the effect of membrane bending stiffness (Pozrikidis (2001)) and membrane prestress (Lac & Barthès-Biesel (2005)). The behavior of the capsule is also highly sensitive to the initial shape conditions. Bagchi & Kalluri (2009) showed that oblate capsules in shear flows can experience tumbling (flipping of the capsule) or swinging (angular oscillation of the capsule around its main direction) mode motions, depending on the viscosity ratio and capillary number.

An intensive effort has been also carried out to understand the dynamics of capsules in complex bounded flows. Leyrat-Maurin & Barthès-Biesel (1994); Quéguiner & Barthès-Biesel (1997); Diaz & Barthès-Biesel (2001) studied in detail the axisymmetric deformation of spherical capsules flowing through cylindrical pores under a steady flow. They showed that capsules acquire a steady parachute shape when the radius is comparable or smaller than the tube radius. Pozrikidis (2005a,b) investigated the motion of different types of capsules flowing through a tube. In agreement with experimental observations (see Goldsmith (1971)), the simulations showed that spherical capsules, initially placed out of the centereline of the tube, migrate towards the centerline whilst at the same time exhibit tank-treading. This effect leads to a reduction in the apparent viscosity flow and flow resistance. Doddi & Bagchi (2008) analyzed this migration phenomenon by studying a capsule in a tube subject to a plane Poiseuille flow, and found that the migration velocity decays with the distance to the lateral wall while it increases with the capillary number. Similar findings have been reported under different wall-bounded flows by Pranay et al. (2012); Shi et al. (2012); Singh et al. (2014); Nix et al. (2014, 2016). The motion of capsules through tube constrictions and non-cylindrical tubes have also been investigated, see for example Zhao et al. (2010); Hu et al. (2012); Kuriakose & Dimitrakopoulos (2013); Park & Dimitrakopoulos (2013); Schaaf & Stark (2017); Luo & Bai (2017); Maestre et al. (2017).

However, in nature and in many bioengineering applications, capsules are usually confined in conduits and subjected to unsteady flows. This unsteadiness is inherent in biological systems such as the heart pulse, respiration or the spontaneous contraction of arteries and micro-vessels (known as the vasomotion effect). In lab-systems, microcapsules are usually driven through microchannels for transport, filtering or other purposes. In these systems, the flow is usually produced by peristaltic pumps, due to their relative simplicity and easy miniaturization. These devices consist of a series of diaphragms, which actuate similarly as a muscle contraction and generate a pulsatile flow (the reader is referred to Lin et al. (2006) for more details about peristaltic micropumps). In these systems, the capsule is driven by a net positive pulsatile flow with a high frequency. Under this condition, the capsule suffers cyclic deformations that can even cause the fail of the membrane. Focused on drug-delivery systems, and inspired by these cycles of traction and relaxation of the capsule, new techniques are being investigated as a controlled way to release the internal liquid (see Long et al. (2015)). During the stretching period of the capsule, the liquid is ejected through the pores of the membrane. The release rate can then be controlled by the frequency and intensity of deformations. This technique allows a better diffusion of the internal liquid than standard techniques based on the rupture of the membrane.

A limited number of works on unsteady flows have been reported in the literature, most of them are focused on unbounded shear flows. Numerical simulations of capsules under sinusoidal shear flows reveal that the behavior of capsules changes with respect to steady flows (see Zhao & Bagchi (2011); Matsunaga et al. (2015); Subramaniam & Gee (2016)). The deformation of spherical capsules increases as the flow frequency is reduced. Matsunaga et al. (2015) found an overshoot phenomenon in spherical capsules (i.e. larger deformations in unsteady flow than in steady

flow) at low frequencies, high capillary numbers and viscosity ratios coupled with oscillations of the main capsule orientation similar to the swing mode. Recently, Zhu et al. (2015) investigated the influence of a near wall. These authors showed that the capsule migrates far away from the wall with a periodic wiggling motion and found optimal values of the capillary number where the migration velocity reaches a maximum value.

The objective of this paper is the analysis of the dynamics of confined deformable capsules in bounded unsteady flows, which is typically found in nature and in many bioengineering applications. In particular, we investigate the motion of capsules in a pipe under a pulsatile flow with a non-null average flow velocity. To the authors' knowledge this physical situation has not previously reported in the literature. The capsule is placed out of the centerline of the tube, which breaks the axisymmetry of the problem. We consider the membrane is an infinitely thin hyperelastic material that follows a Skalak model (see Skalak et al. (1973)). We analyze the influence of the capillary number, flow frequency and amplitude of the pulse in the response of the capsule. A coupled three-dimensional isogeometric boundary-finite element method (BEM-FEM) approach, based on the T-spline framework, is used in the simulations. This approach provides stable and accurate results as shown in Maestre et al. (2017).

This work is structured as follows. In Section 2 we present the hydrodynamic and mechanical formulation of the problem, a brief explanation of the numerical method utilized and the description and initial configuration of the problem considered. In Section 3 we discuss the results and in Section 4 we summarise and conclude.

2. Problem statement

2.1. Formulation of the problem

We analyze the behavior of a capsule flowing in a microchannel. The microchanel is a long cylindrical tube, defined by the boundary Γ_T, through which an external fluid, Ω_1, flows. The capsule is made of a thin membrane, represented by Γ_C, and encloses an internal fluid, Ω_2 . This capsule can move and deform freely due to the action of the external flow. The motion of the capsule is then a consequence of the complex fluid-structure-fluid interaction. Fig. 1 shows an illustration of the problem. Since the hydrodynamic and mechanical formulation of the problem is well known (see for example Ramanujan & Pozrikidis (1998); Pozrikidis (2003, 2005b)), we explain it briefly.

As is habitual in microfluidics, the Reynolds number is very low and the fluids (internal and external fluids) can be described by the Stokes equation as,

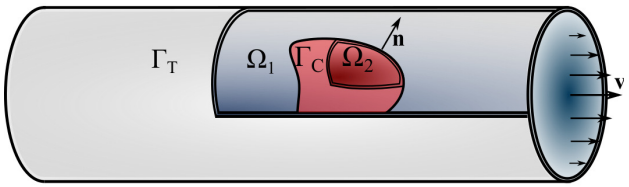

Figure 1: Sketch of the problem

$$\begin{cases} \nabla \cdot \mathbf{v}_i = 0 \\ \nabla \cdot \boldsymbol{\sigma}_i = -\nabla p_i + \mu_i \nabla^2 \mathbf{v}_i = 0 \end{cases} \qquad \text{in } \Omega_i,\ i = 1, 2 \tag{1}$$

where $\boldsymbol{\sigma}_i$ is the fluid stress tensor, $\mathbf{v}_i$ is the fluid velocity, p_i is the pressure and μ_i is the viscosity in the fluid domain Ω_i.

In this study, both fluids are assumed to be incompresible and Newtonian with the same properties. No-slip conditions are considered on the membrane and tube. The fluid velocity is continuous across both sides of the membrane, whereas the fluid stress is discontinuous. The boundary conditions on the membrane can then be written as,

$$\begin{cases} \mathbf{v}_1 = \mathbf{v}_2 \\ \mathbf{t}_C = (\boldsymbol{\sigma}_1 - \boldsymbol{\sigma}_2)\mathbf{n} \end{cases} \qquad \text{on } \Gamma_C \tag{2}$$

where $\mathbf{n}$ is the unit outward normal to the capsule and $\mathbf{t}_C$ is known as jump.

The behavior of the capsule depends strongly on the mechanical characteristics of the membrane. The membrane can suffer large deformations, changing the shape of the capsule. In accordance with many studies (see for example Diaz & Barthès-Biesel (2001); Lefebvre & Barthès-Biesel (2007); Dodson III & Dimitrakopoulos (2009)), we consider the membrane as an isotropic thin hyperelastic shell with negligible bending resistance. Using a bi-dimensional description of the membrane, the local equilibrium on the capsule is given by the equation,

$$\nabla_s \cdot \boldsymbol{\tau} + \mathbf{t}_C = 0 \quad \text{on } \Gamma_C \tag{3}$$

where ∇_s is the surface divergence and $\boldsymbol{\tau}$ is the in-plane Cauchy stress tensor. This tensor can be written in terms of a strain energy function, Ψ, as follows,

$$\boldsymbol{\tau} = \frac{\partial \Psi(\boldsymbol{F})}{\partial \boldsymbol{F}} \frac{\boldsymbol{F}^T}{J_s} \tag{4}$$

where $\boldsymbol{F}$ is the deformation gradient and $J_s = |\boldsymbol{F}|$ is the surface dilatation. Note that inertial effects have been neglected due to the small thickness of the membrane.

Several constitutive laws, that govern the mechanical behavior of the membrane, have been proposed in the literature (see for instance Barthès-Biesel et al. (2002); Lac et al. (2004)), but two of them are used more frequently: the Neo-Hookean model and the model developed by Skalak et al. (1973). The Neo-Hookean model is usually employed in artificial capsules with a ruber-like behavior. The Skalak model was initially formulated for RBCs and it has also been applied satisfactorily to alginate-based biocapsules (Lefebvre & Barthès-Biesel (2007)). This type of capsules is employed typically in many biological applications, for example in drug delivery systems, due to its biocompatibility properties (see Nahar et al. (2017)). In this work, we use the Skalak model. The energy function for a bi-dimensional membrane is defined as,

$$\Psi^{Sk} = \frac{G_s}{4}\left(I_1^2 + 2I_1 - 2I_2 + CI_2^2\right) \tag{5}$$

where G_S is the shear modulus, C is a dimensionless coefficient that relates the area dilation to the shear modulus, and $\{I_1, I_2\}$ are the two strain invariants. This model follows a strain-hardening behavior and for large values of $C >> 1$ the membrane becomes almost area incompressible.

2.2. Numerical method

In this study, an isogeometric BEM-FEM approach is used to analyze the dynamics of deformable capsules in confined flows. The Stokes flows are solved using BEM, whereas a weak formulation, based on the FEM, is applied to the membrane. Both methods are formulated in the context of isogeometrical analysis (IgA) T-spline. Since this approach has been presented previously in Maestre et al. (2017), we only describe it briefly.

The velocity of the capsule is given by the boundary integral equation (BIE) applied to the membrane interface,

$$\mathbf{v}_C(\mathbf{x}) = -\frac{1}{8\pi\mu}\left[\int_{\Gamma_C} \mathbf{G}(\mathbf{x})\mathbf{t}_C d\Gamma + \int_{\Gamma_T} \mathbf{G}(\mathbf{x})\mathbf{t}_T^D d\Gamma\right] + \mathbf{v}^\infty(\mathbf{x}) \qquad \mathbf{x} \in \Gamma_C \tag{6}$$

where $\mathbf{G}$ is the free space Green's function of the Stokes flow (see Pozrikidis (2002)), $\mathbf{t}_T^D$ is the disturbed fluid traction vector on the tube and $\mathbf{v}^\infty$ is the undisturbed flow across the tube. Note that the flow is assumed to be the superposition of an undisturbed flow (denoted by the superscript ∞) and a disturbed flow (denoted by the superscrip D), such that the velocity and traction are defined to be $\mathbf{v} = \mathbf{v}^\infty + \mathbf{v}^D$ and $\mathbf{t} = \mathbf{t}^\infty + \mathbf{t}^D$, respectively. The undisturbed flow corresponds to the flow across the tube without considering the presence of the capsules and the disturbed flow is produced due to the movement of the capsule in the tube. This technique simplifies the formulation and an analytical solution of the undisturbed flow can be used . Interested readers are referred to Pozrikidis (2005b) for more details.

The traction on the tube is computed by applying the BIE on the tube boundary as follows,

$$\int_{\Gamma_T} \mathbf{G}(\mathbf{x})\mathbf{t}_T^D d\Gamma = -\int_{\Gamma_C} \mathbf{G}(\mathbf{x})\mathbf{t}_C d\Gamma \qquad \mathbf{x} \in \Gamma_T. \tag{7}$$

The jump stress term, $\mathbf{t}_C$, can be calculated by applying the principle of virtual work to the membrane. This principle can be written as,

$$\int_{\Gamma_C} \delta\mathbf{u}(\mathbf{x}) \cdot \mathbf{t}_C(\mathbf{x}) d\Gamma = \int_{\Gamma_C} \delta\boldsymbol{e}(\mathbf{x}) : \boldsymbol{\tau}(\mathbf{x}) d\Gamma \qquad \mathbf{x} \in \Gamma_C \tag{8}$$

where $\delta\mathbf{u}(\mathbf{x})$ is a virtual displacement and $\delta\mathbf{e}(\mathbf{x})$ is the virtual Euler-Almansi strain tensor (see Holzapfel (2000)).

Under the isogeometric paradigm, the geometry and the physical variables, involved in the Eqs. (6), (7) and (8), are defined in a finite dimensional space described by T-spline basis functions. This can can be written as,

$$\Phi(\mathbf{x}) = \sum_{A=1}^{m_{cp}} R_A(\mathbf{x}) \Phi_A \tag{9}$$

where Φ is referred to the geometrical and physical variables, $R_A(\mathbf{x})$ is the T-spline basis functions, Φ_A are the values of discretized variables at the control points and m_{cp} is the number of basis function (see Fig. 2).

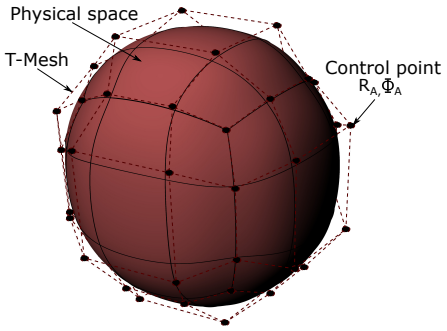

Figure 2: T-spline representation of a spherical capsule. The T-spline surface (or physical space) is defined by a T-spline mesh (T-mesh), which is made of control points. Each control point has associated a T-spline base and physical variable.

The T-spline basis provides a high-order of approximation (cubic rational polynomials) and continuity (until C^2). These properties make the method accurate and stable even under large movements of the capsule, as has been demonstrated by Maestre et al. (2017). Moreover, complex geometric models can be constructed easily through a direct link with computer aided design softwares. For more details about the use of T-splines as a basis for the IGA, the reader is referred to Bazilevs et al. (2010); Scott et al. (2011, 2013).

The interface of the capsule is tracked by the differential equation,

$$\mathbf{v}_C = \frac{d\mathbf{x}}{dt} \qquad \mathbf{x} \in \Gamma_C \tag{10}$$

A second order implicit time integration scheme (Crank-Nicolson scheme) with an adaptive time step is used to convect the capsule interface. This strategy improves the stability of the approach and balances computational cost and accuracy. Additionally, a volume constrain equation with null flux across the membrane is enforced to reduce the numerical errors during the simulation.

2.3. Set-up

We consider an initial spherical capsule filled with a fluid with the same viscosity as the flowing fluid in the tube. The capsule follows a Skalak law with $C = 1$. The tube is a cylinder of radius R_T and its centerline is taken coincident with the x_1-axis. The ratio between the radius of the capsule and the radius of the tube is set to $\delta = R_C/R_T = 0.5$. The center of the capsule is contained in the central section of the tube and it is placed at a radial distance, $r_C = 0.25R_T$, from the centerline. The tube has a length $L_T = 2\pi R_T$, which is large enough to assume that the contribution of the disturbed flow velocity at the inlet and outlet is negligible, whereas the disturbed flow stress can be assumed practically constant in both sections (see Pozrikidis (2005b); Maestre et al. (2017)). where Q^∞ is the instantaneous flow rate.

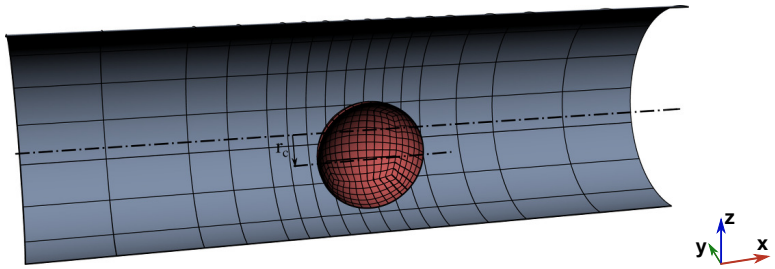

Figure 3: T-spline representation for the non-axisymmetric problem of a capsule flowing through a cylindrical tube. For clarity, only half of the model is represented.

The capsule is discretized using an unstructured T-spline mesh with 602 control points and the tube is built with a structured T-spline mesh with 19×24 control points. A refinement is applied around the central region of the tube to capture with good accuracy the variation of the traction vector on the pipe wall (see Fig. 3).

In this paper, we consider a pulsatile flow with non-null average velocity. The undisturbed flow inside the tube is governed by the Womersley solution (Womersley (1955)). In the Stokes regime, the inertial effects are negligible and the solution can be simplified by a periodic Poiseuille flow. The undisturbed flow can then be expressed as,

$$\mathbf{v}^{\infty}(r,t) = [\Delta v(r) cos(\omega t) + v_0(r)]\, \boldsymbol{x}_1 \tag{11}$$

where r is the radial distance measured from the centerline of the tube, $\boldsymbol{x}_1$ is the unit vector in the axial direction, ω is the frequency of the pulse, $\Delta v(r)$ is the radial amplitude of the pulse and $v_0(r)$ is the radial time average velocity. These last two terms obey the parabolic profile of Poiseuille flow, that is, $f(r) = 2f_m(1 - (r/R_T)^2)$ with f_m being the mean velocity in the section. The flow rate across the tube is given by

$$Q^{\infty}(t) = \frac{\Delta P^{\infty}(t)\pi R_T^4}{8\mu L} = \left[\Delta v_m^{\infty} cos(\omega t) + v_{0m}^{\infty}\right]\pi R_T^2 \tag{12}$$

in which $\Delta P^{\infty}(t)$ is the unsteady pressure drop along the tube length and the subscript $(\cdot)_m$ denotes the mean velocity in the section.

We select a representative value for the shear modulus of a bio-artificial capsule $G_s = 6 \cdot 10^{-6} N/m$, fluid viscosity $\mu = 1.2 \cdot 10^{-3} Ns/m^2$, fluid density $\rho = 1.025 g/cm^3$ and average flow velocity within the range $v_{0m}^{\infty} = [0.375 - 6.00] mm/s$. Considering a representative radius of the pipe $R_T = 10\mu m$, the Reynolds number is in the range of $Re = [0.0032, 0.0513]$. We carried out several simulations for the range of capillary numbers $Ca = [0.075 - 1.2]$, amplitudes of the pulse $\Delta v_m^{\infty}/v_{0m}^{\infty} = [0, 1/3, 2/3]$ and angular velocities $\omega' = \omega R_T / v_{0m}^{\infty} = [1/6\pi - 6\pi]$. The capillary number is a dimensionless parameter that relates the fluid stress on the membrane with the elastic stress. This parameter and the ratio between the radius of the capsule and the radius of the tube determine the behavior of the capsule under a constant flow. In the case of a capsule in a pulsatile flow, it can be defined as,

$$Ca = \frac{\mu \overline{Q}^{\infty}}{\pi R_T^2 G_s} \tag{13}$$

where $\overline{Q}^{\infty}$ is the average flow rate in the tube.

In nature, we can find capsules exposed to an internal pressure. There are several causes for this such as the osmotic pressure produced by a different concentration of any substance on both sides of a semi-permeable membrane. This osmotic pressure was found in experimental alginate-based microcapsules (see Sherwood et al. (2003)). We take into account the internal pressure by applying a pre-inflation of the initial spherical capsule from a radius R_{C0} to a radius $R_C = (1 + \alpha)R_{C0}$, which produces a membrane stress given by $\tau_{iso} = 1/2 p_{os} R_C$, where p_{os} is the internal osmotic pressure and α is the expansion coefficient. In this work, we consider a low coefficient $\alpha = 0.025$, according to previous experimental and numerical studies of biocapsules (see Risso et al. (2006); Lefebvre & Barthès-Biesel (2007). The interested reader is referred to Lac & Barthès-Biesel (2005); Lefebvre & Barthès-Biesel (2007) for more details about prestressed capsules.

2.4. Validation

First, we checked the validity of the present model by simulating a capsule flowing in a pipe under a constant flow. The capsule is initially spherical and it is placed at the centerline of the tube. This problem was analyzed by Lefebvre & Barthès-Biesel (2007) using a 2D axisymmetric BEM model. These authors found that the capsule evolves to a steady configuration, in which the capsule acquires a parachute shape, and they studied the influence of different parameters in capsule deformation.

A 3D T-Spline-based isogeometric model, as previously described in Section 2.3, is used. The amplitude of the imposed flow is set at $\Delta v_m^\infty = 0$ and the initial capsule position is given by $r_C = 0$. Fig. 4 shows the deformation of a Skalak capsule at the steady state for the capillary number $Ca = 0.06$, $\alpha = 0.025$ and $\delta = 0.8$ and 0.9. The agreement between the capsule shape predicted by the present model and that reported by Lefebvre & Barthès-Biesel (2007) is very good.

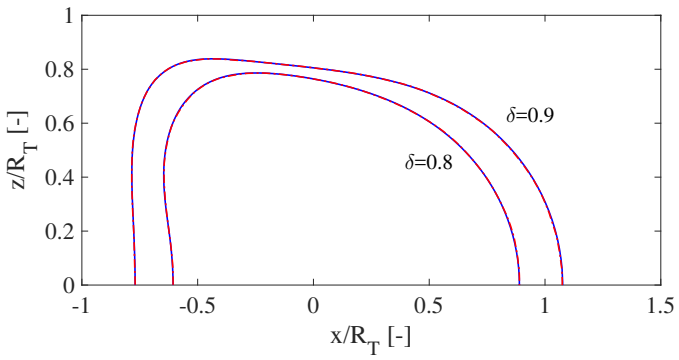

Figure 4: Profile of a Skalak deformable capsule ($C = 1$) flowing in a cylindrical tube by the action of constant flow for $Ca = 0.06$, $\delta = 0.8$ and 0.9, $r_C = 0$ and $\alpha = 0.025$. Only a half of the profile is represented given the axisymmetry of the problem. Present result for a three dimensional model: continuous line; results reported by Lefebvre & Barthès-Biesel (2007) for an axisymmetric model: dashed-dotted line.

3. Results and discussion

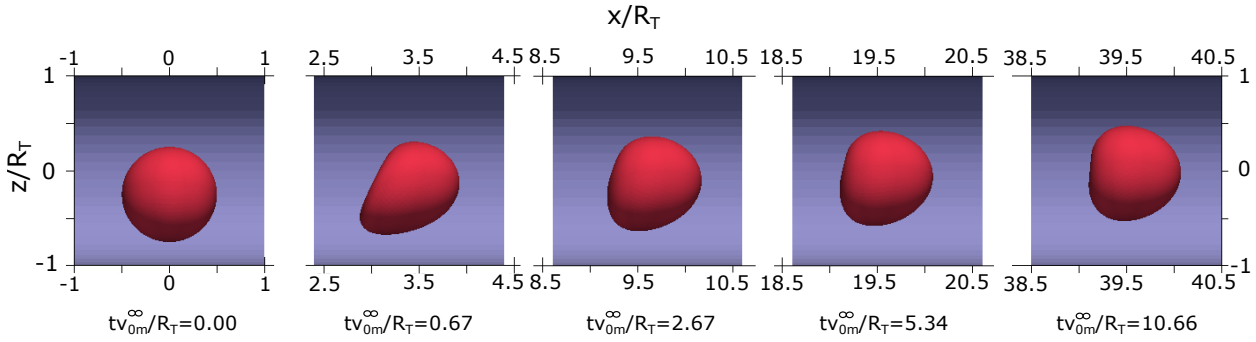

Figure 5: Time evolution of the lateral view of a capsule in a pulsatile flow with $Ca = 0.15$, $\Delta v_m^\infty / v_{0m}^\infty = 2/3$ and $\omega' = 2/3\pi$.

In this section, we analyze the behavior of a spherical Skalak capsule, as described in Section 2.3, moving in a pipe under a pulsatile flow. Fig. 5 shows the time evolution of a capsule in a flow with $Ca = 0.15$, $\Delta v_m^\infty / v_{0m}^\infty = 2/3$ and $\omega' = 2/3\pi$. We found an initial period in which the capsule is rapidly deformed and it adopts a non-symmetric shape. Then, the capsule asymptotically migrates to the centerline of the tube. In this way, the capsule exhibits a quasi-periodic deformation due to the pulsating character of the flow. Fig 6 shows the typical oscillations of the

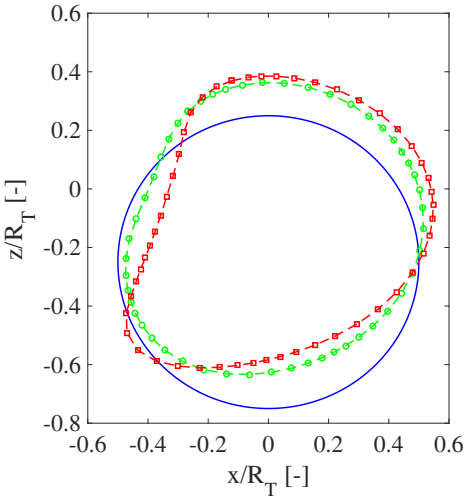

Figure 6: Evolving shape of a capsule in a pulsatile flow with $Ca = 0.15$, $\Delta v_m^\infty / v_{0m}^\infty = 2/3$ and $\omega' = 2/3\pi$ at times $t v_{0m}^\infty / R_T = 0.00$ (solid line), 2.34 (circles) and 3.00 (squares) corresponding to the initial, and minimum and maximum surface deformation in a cycle. The meridian plane is represented and the frame follows the volume center of the capsule along the x_1-direction.

capsule corresponding to the maximum and minimum surface deformation in a cycle. As the capsule gets closer to centerline of the tube, it acquires an oscillating axisymmetric parachute shape.

The surface area variation of the capsule is a representative parameter to measure the global surface deformation, since it is related to the strain in the membrane. This quantity measures the change of the surface area from the initial configuration (after the pre-inflation) to the actual configuration ($\Delta s/s_0 = (s(t) - s_0(t=0))/s_0(t=0)$ with s being the total surface area). Figs. 7a, 7b and 7c, show the time evolution of the surface deformation of a capsule in a pulsatile flow for different values of the amplitude of the pulse, frequency and capillarity, respectively. In the case of zero flow amplitude, this is, steady flow (see Fig. 7a), we observe an initial transient period where a maximum area change is quickly reached and then the capsule slowly deforms as it migrates to the centerline of the tube. For amplitudes of pulsatile flow larger than zero, the surface deformation acquires a quasi-periodic behavior that oscillates around the response of the constant flow and with the same frequency as the imposed pulsatile flow.

The surface deformation exhibits a strong dependence on the stiffness of the membrane and on the frequency of the pulsatile flow. As shown in Fig. 7b, the amplitude of the surface deformations decays with the frequency because the capsule has less time to deform in each cycle. The influence of the capillarity is illustrated in Fig. 7c where the area variation is depicted for three different capillary numbers. The amplitude of the oscillation, as well as the average trend (measured as the temporal moving average with a span of a cycle), increases with the capillarity. The capsule becomes relatively softer and it suffers a larger elongation along the flow direction (see Fig. 8). Although the inertia effects are negligible, it is interesting to observe the time delay between the surface deformation and the pulsatile flow. This delay slightly increases for higher values of the capillary number and the frequency.

Fig. 9 clearly shows the influence of the frequency of the pulsatile flow and the capillary number on the surface deformation of the capsule. Fig. 9a shows that at low frequency, the amplitude of the surface deformation tends asymptomatically towards a maximum value whereas at high frequencies it goes to zero. On the other hand (Fig. 9b), the surface deformation (the amplitude and the average trend) increases monotonically with the capillary number due to the lower stiffness of the membrane. Moreover, at low frequency of the pulsatile flow, we found an overshooting phenomenon of the capsule (see Fig. 10). This phenomenon creates a larger surface deformation of the membrane than the corresponding deformation in a constant flow with the flow velocity equal to the maximum flow velocity of the pulsatile flow. The overshooting was also reported by Matsunaga et al. (2015) in an unbounded oscillating shear flow.

As it has been observed experimentally and numerically, an off-centered capsule migrates towards centerline of the tube under a constant flow (see for example Goldsmith (1971); Helmy & Barthès-Biesel (1982); Pozrikidis (2005b);

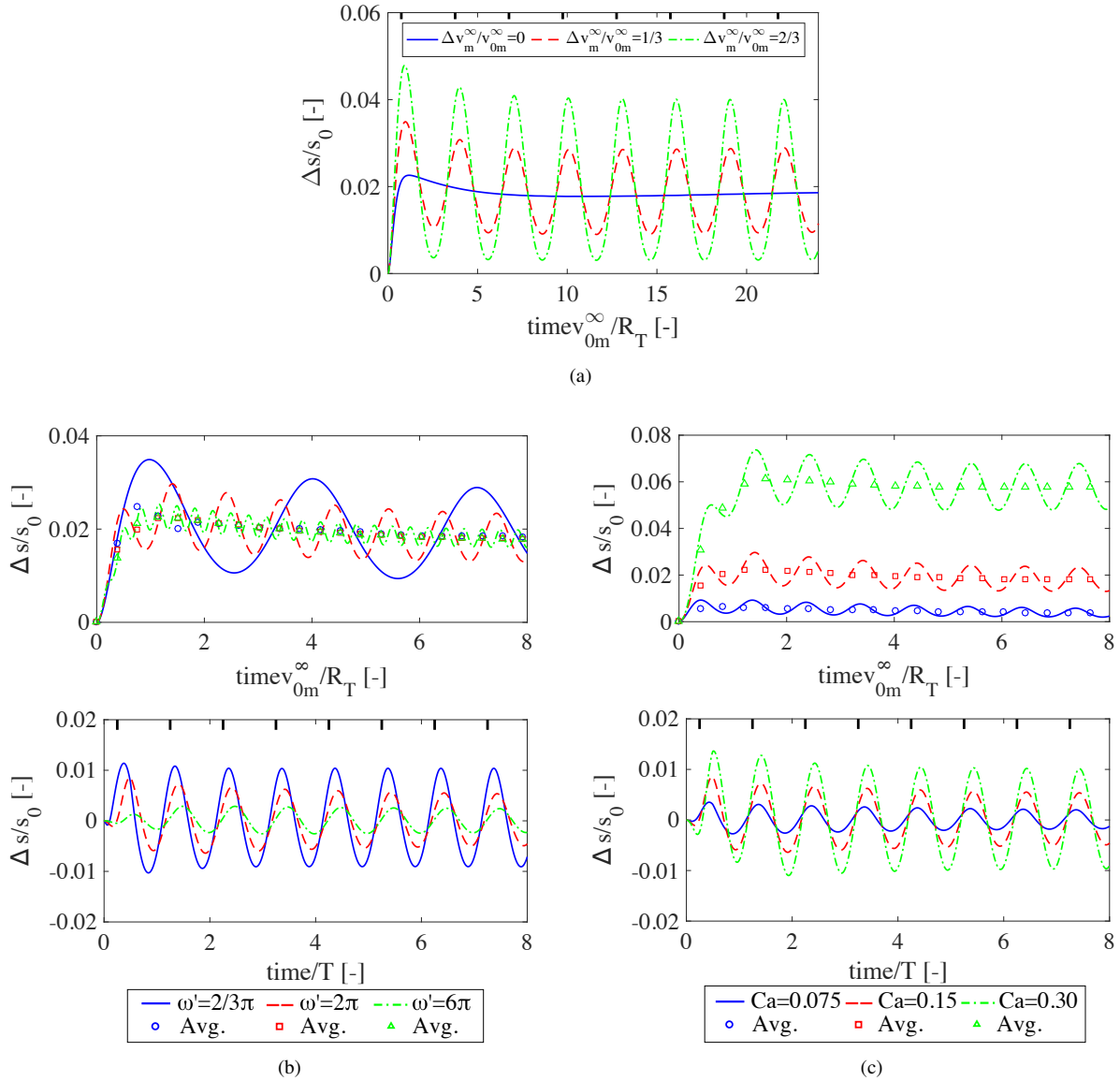

Figure 7: (a) Time evolution of the area variation of the capsule in pulsatile flow with $Ca = 0.15$, $\omega' = 2/3\pi$ and three different amplitudes; (b) in a pulsatile flow with amplitude $\Delta v_m^\infty / v_{0m}^\infty = 1/3$, $Ca = 0.15$, and various frequencies (top: as a function of the dimensionless time tv_{0m}^∞ / R_T; and bottom: as function of the dimensionless time t/T and subtracting the average term); and (c) in a pulsatile flow with amplitude $\Delta v_m^\infty / v_{0m}^\infty = 1/3$, $\omega' = 2\pi$ and different capillarities (top: as a function of the dimensionless time tv_{0m}^∞ / R_T; and bottom: as a function of the dimensionless time t/T and subtracting the average term). The vertical marks along the top x-axis denote the maximum peaks of the pulsatile flow. The average is computed as a moving average with the span of a cycle.

Coupier et al. (2008); Shi et al. (2012); Singh et al. (2014); Zhu et al. (2015); Maestre et al. (2017), . This phenomenon is due to the deformability of the capsule and the influence of near walls in the capsule deformation (see Nix et al. (2016)). Note that a solid neutral buoyancy capsule always is maintained parallel to the flow direction. Doddi & Bagchi (2008) found that the migration velocity of a deformable capsule depends on the distance to the pipe wall, the capillarity as well as the relative pipe-capsule size for a planar steady Poiseulle flow. Fig. 11 shows the migration velocity of the capsule for different frequencies of the pulse as a function of the radial distance to centerline of the tube. We found that the migration velocity (after an initial transient period) decreases as the capsule get closer to the

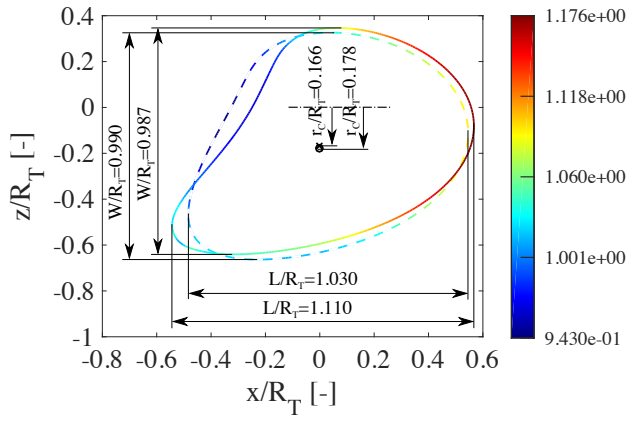

Figure 8: Surface dilatation ($J_{s0} = \frac{ds}{ds_0}$) of a capsule in a pulsatile flow with amplitude $\Delta v_m^\infty / v_{0m}^\infty = 1/3$, frequency $\omega' = 2\pi$ and $Ca = 0.15$ (solid line) and $Ca = 0.30$ (dashed line) at the time $tv_{0m}^\infty / R_T = 3.750$. The circle and cross markers denote the centroid for $Ca = 0.15$ and $Ca = 0.30$, respectively.

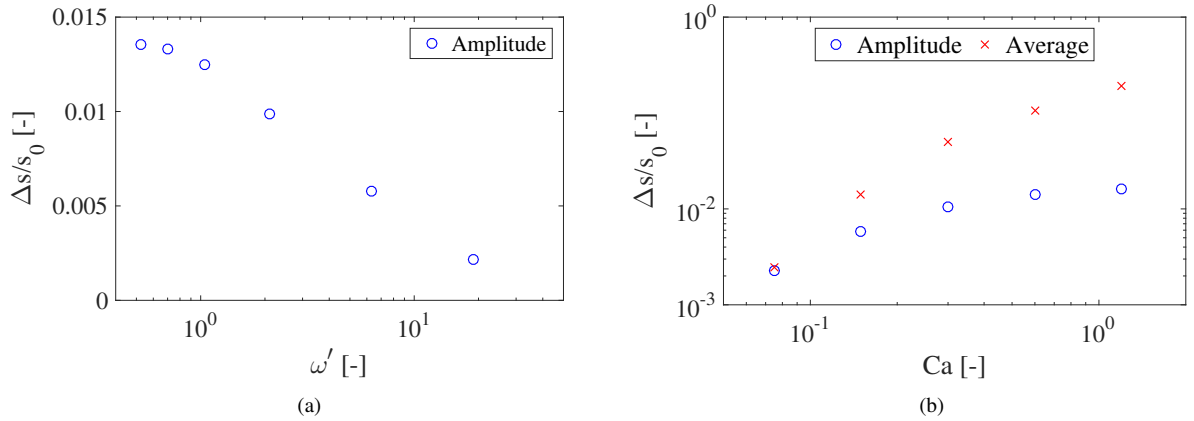

Figure 9: a) Area variation of a capsule in a pulsatile flow with amplitude $\Delta v_m^\infty / v_{0m}^\infty = 1/3$, $Ca = 0.15$ and for a range of frequencies $\omega' = [1/6-6]\pi$. b) Area variation for a capsule in a pulsatile flow with amplitude $\Delta v_m^\infty / v_{0m}^\infty = 1/3$, frequency $\omega' = 2\pi$ and for a range of capillary numbers $Ca = [0.075 - 1.2]$. Results obtained at $tv_{0m}^\infty / R_T = 9$.

centerline with an oscillatory behavior. The decrease of the average trend and amplitude of the oscillations follow a power function with the same exponent. This degree is practically insensitive to the frequency of the pulse. As observed previously in the deformation of the capsule, the amplitude of the oscillations get larger for lower frequency values, which reveals the link between both parameters.

The influence of the capillary number on the migration velocity for a pulsatile flow is shown in Fig. 12. In consonance with the surface deformation, the capsule increases the migration velocity for higher values of the capillarity. It also is interesting to note the delay of the oscillations for the different values of the capillary number. This delay is due to their difference in the average migration velocity. As shown in Fig. 13, the average trend increases monotonically with the capillary number. However, the amplitude of the oscillation exhibits a maximum close to $Ca = 0.3$. This finding is in agreement with Zhu et al. (2015), who also found the same behavior for a capsule in a wall-bounded shear oscillating flow.

Fig. 14 shows the time evolution of the slip velocity for various values of frequency and capillarity. This velocity is defined as the difference between the horizontal velocity of the undisturbed flow at the position of the centroid of the capsule and the horizontal velocity of the capsule ($v_{CS} = (v_1^\infty(r = x_3^{vc}) - v_1^{vc})/v_{0m}^\infty$). The slip velocity is always positive.

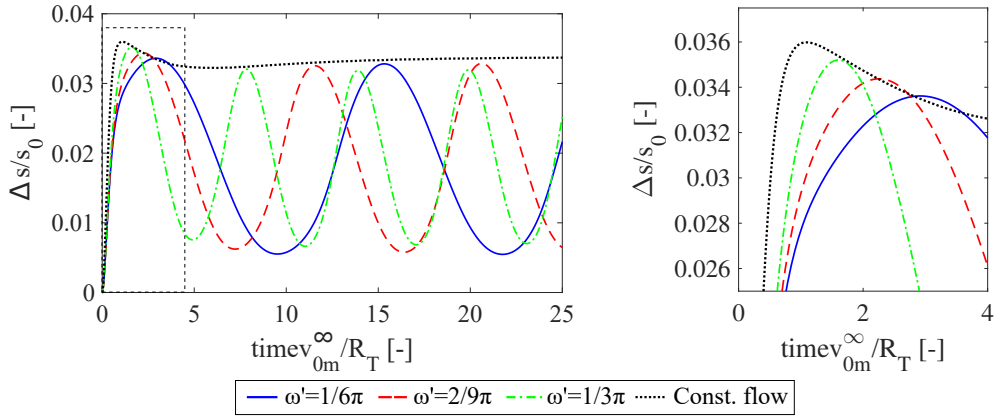

Figure 10: Overshooting response of a capsule in a pulsatile flow with amplitude $\Delta v_m^\infty / v_{0m}^\infty = 1/3$, $Ca = 0.15$ and different frequencies.

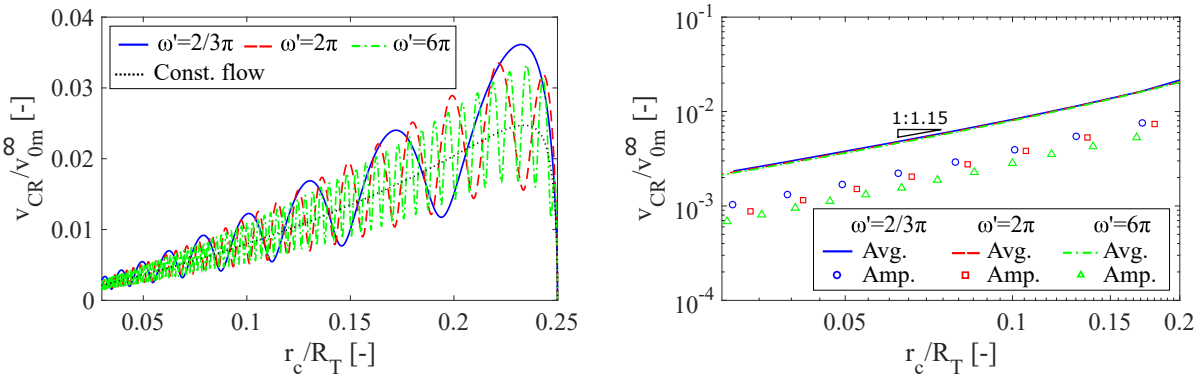

Figure 11: (a) Evolution of the migration velocity (defined as $v_{CR} = -\frac{dr_C}{dt}$) as function of the radial distance to the centerline of a capsule in pulsatile flow with $Ca = 0.15$, amplitude $\Delta v_m^\infty / v_{0m}^\infty = 1/3$ and different values of the frequency. (b) Evolution of the average trend and amplitude of the migration velocity for this capsule under same conditions using log-log scales.

The capsule moves at a lower velocity than the flow. This velocity asymptotically decreases as the capsule moves to the centerline. We observed a reduction of the amplitude of the oscillations with the capillary number and frequency. Note that in all the cases, the average slip velocity of the capsule tends towards lower values than the theoretical slip velocity of a neutral buoyancy solid capsule placed at centerline. These values are lower for higher capillarities. The deformation of the capsule favors the horizontal velocity of the capsule.

Due to the initial off-centered position of the capsule, the flow generates a torque on the membrane and as consequence it suffers a tank-treading effect. Fig. 15a depicts the distribution of the tangential velocity (v_t) on the meridian plane of the membrane after subtracting the radial and horizontal velocity of the whole capsule. The membrane has a net tangential velocity in the clockwise direction, although the direction is determined by the position of the capsule in the tube (i.e. if it is under the centerline or over it). Given the pulsatile character of the flow, the rotation also exhibits an oscillatory behavior. This is illustrated in Fig. 15b where the mean tangential velocity on the membrane (v_{CT}) is shown. Initially, the mean tangential velocity is close to the theoretical value computed for a neutral buoyant solid sphere placed at a distance $r_C = 0.25R_T$ from the centerline. The time average value asymptotically tends to decay with time as well as the amplitude of the oscillations. This is attributed to the migration of the capsule to the centerline. In fact, for softer capsules, we found a larger reduction of the tank-treading effect due to the faster migration process. In the limit, when the capsule reaches the centerline of the tube, the shape of the capsule becomes

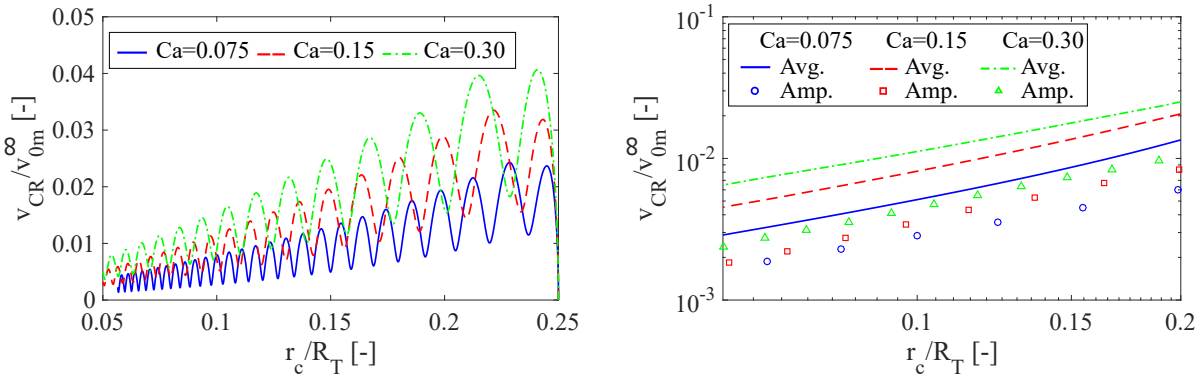

(a) (b)

Figure 12: (a) Evolution of the migration velocity as function of the radial distance to the centerline of a capsule in pulsatile flow with amplitude $\Delta v_m^{\infty}/v_{0m}^{\infty} = 1/3$, $\omega' = 2\pi$ and different capillarities. (b) Evolution of the average trend and amplitude of the migration velocity for this capsule under same conditions and using a log-log scales.

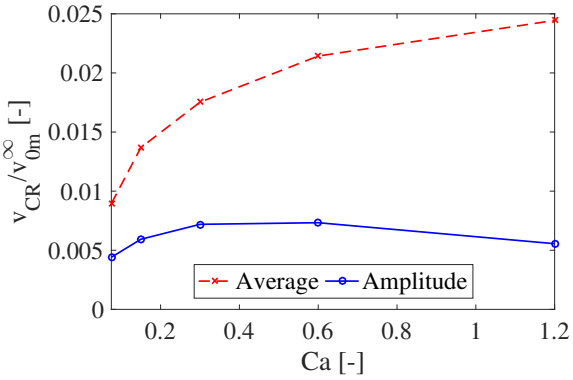

Figure 13: Migration velocity of a capsule (at $r_C = 0.15$) in a pulsatile flow with amplitude $\Delta v_m^{\infty}/v_{0m}^{\infty} = 1/3$, frequency $\omega' = 2\pi$ and for a range of capillary numbers $Ca = [0.075 - 1.2]$

axisymmetric and the tank-treading phenomenon disappears.

As it is well known, the presence of the capsule in the tube causes an increase in the flow resistance that results in an additional pressure drop given by Δp^D. Lefebvre & Barthès-Biesel (2007) found that for an axisymmetric configuration of the capsule and a constant flow, the additional pressure drop is influenced by the relative size and deformability of the capsule. The capsule is primarily elongated in the flow direction, which increases the surrounding viscosity film and consequently the additional pressure drop. The time evolution of the additional pressure drop for different frequencies and capillarities is illustrated in Fig. 16. The amplitude of the oscillations decreases with the frequency because the amplitude of the membrane deformation is also lower. In the case of softer membranes, we observe a lower level of the additional pressure drop because the migration process is dominant. The capsule suffers a larger deformation and consequently migrates more rapidly to the centerline reducing the additional pressure drop as predicted by the theory of solid spheres in a tube. This effect is in agreement with the findings reported by Doddi & Bagchi (2008) for a deformable capsule in a Poiseuille flow.

4. Conclusions

In this study, the behavior of a Skalak artifical capsule flowing through a pipe under a pulsatile flow was numerically investigated using a 3D T-spline-based IgA BEM-FEM approach. The accuracy of the method was previously

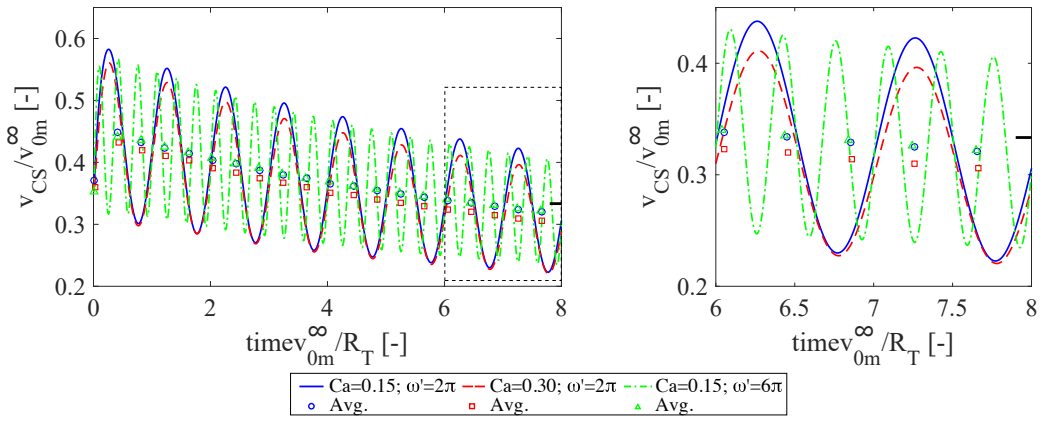

Figure 14: Time evolution of the slip velocity of a capsule in a pulsating flow with an amplitude $\Delta v_m^{\infty}/v_{0m}^{\infty} = 1/3$, different frequencies and capillary numbers. The rigth mark on the y-axis denotes the theoretical slip velocity of a neutral buoyant solid sphere placed at the centerline of a tube.

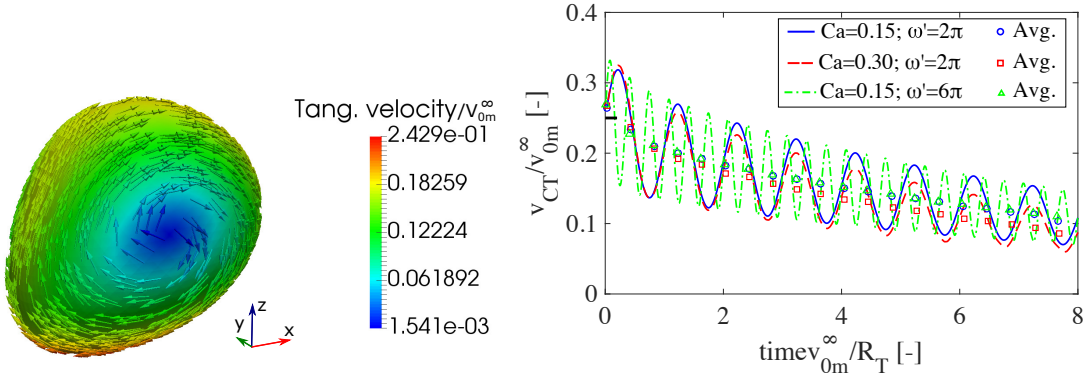

(a) (b)

Figure 15: (a) Tangential velocity distribution on the meridian plane of a capsule (v_t) in a pulsatile flow with $Ca = 0.15$, $\Delta v_m^{\infty}/v_{0m}^{\infty} = 1/3$ and $\omega' = 2\pi$ at time $tv_{0m}^{\infty}/R_T = 2.002$. (b) Time evolution of the mean tangential velocity on the meridian plane of a capsule (v_{CT}) in a pulsating flow for different frequencies and capillarities. The left mark on the y-axis denotes the theoretical tangential velocity of a neutral buoyant sphere placed to a distance $r_C = 0.25R_T$ from the centerline of a tube.

checked by comparing with a benchmark problem and good agreement was obtained.

This configuration can be found in many bioengineering applications, where artificial capsules are driven by the action of mechanical micropumps. We described the influence of the pulsatile flow and the capillary number on the evolution of the capsule. The capsule is deformed and it moves with an oscillatory behavior around its corresponding evolution in a steady flow. We found that the amplitude of deformation of the capsule increase as the frequency is reduced up to a maximum. At relatively low frequencies, the deformation can overshoot the equivalent steady deformation, such that this deformation is larger than the expected deformation. High values of the capillary number involve large deformations of the capsules due to the relative softness of the membrane. We observe that the deformation of the capsule is tightly related to other phenomena. Because of the deformability, an off-centered capsule migrates asymptotically to the centerline of the pipe. Higher deformation of the capsule favors the migration velocity whilst it reduces the slip velocity. As the capsule moves to the centerline, the additional flow resistance, caused by the presence of the capsule, and the tank-treading effect, decreases. This reduction is more pronounced for larger values of the capillary number because of the higher deformation and migration velocity, whilst high flow frequencies reduce the amplitude of the oscillations. Therefore, the control of the frequency and capillarity is crucial in order to regulate

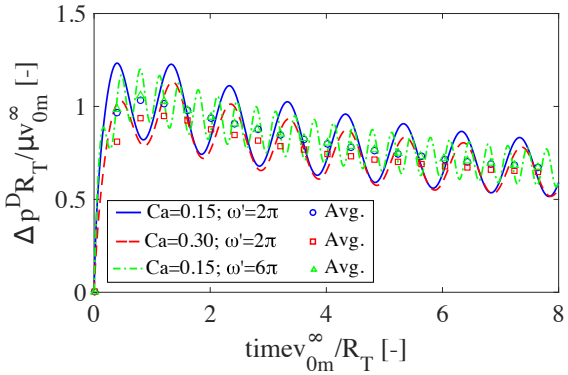

Figure 16: Time evolution of the disturbed pressure drop due to the presence of a capsule in a pulsatile flow with amplitude $\Delta v_m^\infty / v_{0m}^\infty = 1/3$, different frequencies and capillarities.

the deformation and behavior of capsules in pulsatile flows.

Acknowledgments

This study has been supported by the Spanish Ministerio de Economía y Competitividad under project DPI2016-75791-C2-1-P. M. A. Scott was supported by AFOSR Grant FA9550-14-1-0113. This support is gratefully acknowledged.

References

Bagchi, P., & Kalluri, R. M. (2009). Dynamics of nonspherical capsules in shear flow. *Phys. Rev. E*, *80*, 016307.

Bansode, S. S., Banarjee, S. K., Gaikwad, D. D., Jadhav, S. L., & Thorat, R. M. (2010). Microencapsulation: a review. *International Journal of Pharmaceutical Sciences Review and Research*, *1*, 38–43.

Barthès-Biesel, D. (2016). Motion and Deformation of Elastic Capsules and Vesicles in Flow. *Annual Review of Fluid Mechanics*, *48*, 25–52.

Barthès-Biesel, D., Diaz, A., & Dhenin, E. (2002). Effect of constitutive laws for two-dimensional membranes on flow-induced capsule deformation. *Journal of Fluid Mechanics*, *460*, 211–222.

Bazilevs, Y., Calo, V. M., Cottrell, J. A., Evans, J. A., Hughes, T. J. R., Lipton, S., Scott, M. A., & Sederberg, T. W. (2010). Isogeometric analysis using T-splines. *Computer Methods in Applied Mechanics and Engineering*, *199*, 229–263. Cited By 0.

Carin, M., Barthès-Biesel, D., Edwards-Lévy, F., Postel, C., & Andrei, D. C. (2003). Compression of biocompatible liquid-filled HSA-alginate capsules: Determination of the membrane mechanical properties. *Biotechnology and bioengineering*, *82*, 207–212.

Casanova, F., & Santos, L. (2016). Encapsulation of cosmetic active ingredients for topical application–a review. *Journal of microencapsulation*, *33*, 1–17.

Chu, T., Salsac, A.-V., Leclerc, E., Barthès-Biesel, D., Wurtz, H., & Edwards-Lévy, F. (2011). Comparison between measurements of elasticity and free amino group content of ovalbumin microcapsule membranes: discrimination of the cross-linking degree. *Journal of colloid and interface science*, *355*, 81–88.

Coupier, G., Kaoui, B., Podgorski, T., & Misbah, C. (2008). Noninertial lateral migration of vesicles in bounded Poiseuille flow. *Physics of Fluids (1994-present)*, *20*, 111702.

Diaz, A., & Barthès-Biesel, D. (2001). Entrance of a bioartificial capsule in a pore. *Computer Modeling in Engineering and Sciences*, *3*, 321–338.

Doddi, S. K., & Bagchi, P. (2008). Lateral migration of a capsule in a plane Poiseuille flow in a channel. *International Journal of Multiphase Flow*, *34*, 966–986.

Dodson III, W. R., & Dimitrakopoulos, P. (2009). Dynamics of strain-hardening and strain-softening capsules in strong planar extensional flows via an interfacial spectral boundary element algorithm for elastic membranes. *Journal of Fluid Mechanics*, *641*, 263–296.

Fischer, T., & Schmid-Schönbein, H. (1978). Tank tread motion of red cell membranes in viscometric flow: behavior of intracellular and extracellular markers (with film). In *Red Cell Rheology* (pp. 347–361). Springer.

Fischer, T. M., Stohr-Lissen, M., & Schmid-Schonbein, H. (1978). The red cell as a fluid droplet: tank tread-like motion of the human erythrocyte membrane in shear flow. *Science*, *202*, 894–896.

Goldsmith, H. L. (1971). Red cell motions and wall interactions in tube flow. In *Federation Proceedings* (pp. 1578–1590). volume 30.

Gonzalez-Pujana, A., Orive, G., Pedraz, J. L., Santos-Vizcaino, E., & Hernandez, R. M. (2018). Alginates and their biomedical applications. chapter Alginate Microcapsules for Drug Delivery. (pp. 67–100). Springer Series in Biomaterials Science and Engineering volume 11.

Helmy, A., & Barthès-Biesel, D. (1982). Migration of a spherical capsule freely suspended in an unbounded parabolic flow. *Journal de Mécanique théorique et appliquée*, *1*, 859–880.

Holzapfel, G. A. (2000). *Nonlinear Solid Mechanics: A Continuum Approach for Engineering*. John Wiley & Sons Ltd.
Hu, X.-Q., Salsac, A.-V., & Barthès-Biesel, D. (2012). Flow of a spherical capsule in a pore with circular or square cross-section. *Journal of Fluid Mechanics*, *705*, 176–194.
Husmann, M., Rehage, H., Dhenin, E., & Barthès-Biesel, D. (2005). Deformation and bursting of nonspherical polysiloxane microcapsules in a spinning-drop apparatus. *Journal of colloid and interface science*, *282*, 109–119.
Kuriakose, S., & Dimitrakopoulos, P. (2013). Deformation of an elastic capsule in a rectangular microfluidic channel. *Soft matter*, *9*, 4284–4296.
Lac, E., & Barthès-Biesel, D. (2005). Deformation of a capsule in simple shear flow: effect of membrane prestress. *Physics of Fluids (1994-present)*, *17*, 072105.
Lac, E., Barthès-Biesel, D., Pelekasis, N. A., & Tsamopoulos, J. (2004). Spherical capsules in three-dimensional unbounded Stokes flows: effect of the membrane constitutive law and onset of buckling. *Journal of Fluid Mechanics*, *516*, 303–334.
Lefebvre, Y., & Barthès-Biesel, D. (2007). Motion of a capsule in a cylindrical tube: effect of membrane pre-stress. *Journal of Fluid Mechanics*, *589*, 157–181.
Lefebvre, Y., Leclerc, E., Barthès-Biesel, D., Walter, J., & Edwards-Lévy, F. (2008). Flow of artificial microcapsules in microfluidic channels: A method for determining the elastic properties of the membrane. *Physics of Fluids (1994-present)*, *20*, 123102.
Leyrat-Maurin, A., & Barthès-Biesel, D. (1994). Motion of a deformable capsule through a hyperbolic constriction. *Journal of Fluid Mechanics*, *279*, 135–163.
Lin, Q., Yang, B., Xie, J., & Tai, Y.-C. (2006). Dynamic simulation of a peristaltic micropump considering coupled fluid flow and structural motion. *Journal of Micromechanics and Microengineering*, *17*, 220.
Long, Y., Liu, C., Zhao, B., Song, K., Yang, G., & Tung, C.-H. (2015). Bio-inspired controlled release through compression–relaxation cycles of microcapsules. *NPG Asia Materials*, *7*, e148.
Luo, Z., & Bai, B. (2017). Off-center motion of a trapped elastic capsule in a microfluidic channel with narrow constriction. *Soft Matter*, *13*, 8281–8292.
Maestre, J., Pallares, J., Cuesta, I., & Scott, M. A. (2017). A 3D isogeometric BE-FE analysis with dynamic remeshing for the simulation of a deformable particle in shear flows. *Computer Methods in Applied Mechanics and Engineering*, *326*, 70 – 101.
Matsunaga, D., Imai, Y., Yamaguchi, T., & Ishikawa, T. (2015). Deformation of a spherical capsule under oscillating shear flow. *Journal of Fluid Mechanics*, *762*, 288301.
Nahar, K., Hossain, M. K., & Khan, T. A. (2017). Alginate and its versatile application in drug delivery. *Journal of Pharmaceutical Sciences and Research*, *9*, 606.
Nix, S., Imai, Y., & Ishikawa, T. (2016). Lateral migration of a capsule in a parabolic flow. *Journal of biomechanics*, *49*, 2249–2254.
Nix, S., Imai, Y., Matsunaga, D., Yamaguchi, T., & Ishikawa, T. (2014). Lateral migration of a spherical capsule near a plane wall in stokes flow. *Physical Review E*, *90*, 043009.
Park, S.-Y., & Dimitrakopoulos, P. (2013). Transient dynamics of an elastic capsule in a microfluidic constriction. *Soft matter*, *9*, 8844–8855.
Pieper, G., Rehage, H., & Barthès-Biesel, D. (1998). Deformation of a capsule in a spinning drop apparatus. *Journal of colloid and interface science*, *202*, 293–300.
Pozrikidis, C. (1995). Finite deformation of liquid capsules enclosed by elastic membranes in simple shear flow. *Journal of Fluid Mechanics*, *297*, 123–152.
Pozrikidis, C. (2001). Effect of membrane bending stiffness on the deformation of capsules in simple shear flow. *Journal of Fluid Mechanics*, *440*, 269–291.
Pozrikidis, C. (2002). *A practical guide to boundary element methods with the software library BEMLIB*. CRC Press.
Pozrikidis, C. (2003). Numerical simulation of the flow-induced deformation of red blood cells. *Annals of Biomedical Engineering*, *31*, 1194–1205.
Pozrikidis, C. (2005a). Axisymmetric motion of a file of red blood cells through capillaries. *Physics of fluids*, *17*, 031503.
Pozrikidis, C. (2005b). Numerical simulation of cell motion in tube flow. *Annals of biomedical engineering*, *33*, 165–178.
Pranay, P., Henríquez-Rivera, R. G., & Graham, M. D. (2012). Depletion layer formation in suspensions of elastic capsules in newtonian and viscoelastic fluids. *Physics of Fluids*, *24*, 061902.
Quéguiner, C., & Barthès-Biesel, D. (1997). Axisymmetric motion of capsules through cylindrical channels. *Journal of Fluid Mechanics*, *348*, 349–376.
Ramanujan, S., & Pozrikidis, C. (1998). Deformation of liquid capsules enclosed by elastic membranes in simple shear flow: large deformations and the effect of fluid viscosities. *Journal of Fluid Mechanics*, *361*, 117–143.
Rehage, H., Husmann, M., & Walter, A. (2002). From two-dimensional model networks to microcapsules. *Rheologica acta*, *41*, 292–306.
Risso, F., CollÉ-Paillot, F., & Zagzoule, M. (2006). Experimental investigation of a bioartificial capsule flowing in a narrow tube. *Journal of fluid mechanics*, *547*, 149–173.
Schaaf, C., & Stark, H. (2017). Inertial migration and axial control of deformable capsules. *Soft Matter*, *13*, 3544–3555.
Scott, M. A., Borden, M. J., Verhoosel, C. V., Sederberg, T. W., & Hughes, T. J. R. (2011). Isogeometric finite element data structures based on Bézier extraction of T-splines. *International Journal for Numerical Methods in Engineering*, *88*, 126–156. Cited By 0.
Scott, M. A., Simpson, R. N., Evans, J. A., Lipton, S., Bordas, S. P. A., Hughes, T. J. R., & Sederberg, T. W. (2013). Isogeometric boundary element analysis using unstructured T-splines. *Computer Methods in Applied Mechanics and Engineering*, *254*, 197–221.
Sherwood, J., Risso, F., Collé-Paillot, F., Edwards-Lévy, F., & Lévy, M.-C. (2003). Rates of transport through a capsule membrane to attain donnan equilibrium. *Journal of colloid and interface science*, *263*, 202–212.
Shi, L., Pan, T.-W., & Glowinski, R. (2012). Numerical simulation of lateral migration of red blood cells in Poiseuille flows. *International Journal for Numerical Methods in Fluids*, *68*, 1393–1408.
Singh, R. K., Li, X., & Sarkar, K. (2014). Lateral migration of a capsule in plane shear near a wall. *Journal of Fluid Mechanics*, *739*, 421–443.
Skalak, R., Tozeren, A., Zarda, R. P., & Chien, S. (1973). Strain energy function of red blood cell membranes. *Biophysical Journal*, *13*, 245.
Subramaniam, D. R., & Gee, D. J. (2016). Shape oscillations of elastic particles in shear flow. *Journal of the mechanical behavior of biomedical materials*, *62*, 534–544.
Walter, J., Salsac, A.-V., Barthès-Biesel, D., & Le Tallec, P. (2010). Coupling of finite element and boundary integral methods for a capsule in a

Stokes flow. *International journal for numerical methods in engineering*, *83*, 829–850.
Womersley, J. R. (1955). Method for the calculation of velocity, rate of flow and viscous drag in arteries when the pressure gradient is known. *The Journal of physiology*, *127*, 553.
Zhao, H., Isfahani, A. H., Olson, L. N., & Freund, J. B. (2010). A spectral boundary integral method for flowing blood cells. *Journal of Computational Physics*, *229*, 3726–3744.
Zhao, M., & Bagchi, P. (2011). Dynamics of microcapsules in oscillating shear flow. *Physics of Fluids*, *23*, 111901.
Zhu, L., Rabault, J., & Brandt, L. (2015). The dynamics of a capsule in a wall-bounded oscillating shear flow. *Physics of Fluids (1994-present)*, *27*, 071902.